Explosive Hydrothermal Brecciation; Connecting Chemistry, Emplacement and Exploration (Thomson Formation, Paleoproterozoic, Northeastern, MN)

By

Tanner E. Eischen

A thesis submitted in partial fulfillment of the requirements of the degree of

Bachelor of Arts

(Geology)

at

Gustavus Adolphus College

2017

Explosive Hydrothermal Brecciation; Connecting Chemistry, Emplacement and Exploration (Thomson Formation, Paleoproterozoic, Northeastern, MN)

By

Tanner E. Eischen

Under the supervision of Dr. James Welsh

Abstract

Drill core of an igneous brecciated deposit intruding the Thomson Formation (Paleoproterozoic), related to the Tamarack intrusion, and located along the boundary of Carlton and Aitkin counties (northeastern MN) was sampled for major and trace element study. While economically insignificant itself, this graphitic breccia pipe provides a unique opportunity to study the events leading to brecciation and emplacement in subsurface intrusive settings. Previous work by Hendrickson (2011) suggests a syntectonic model of breccia pipe deposition with both the Tamarack and the Mid-Continent Rift system (MRS), and a breccia matrix petrology more closely resembling that of melted country rock (end-of-hole igneous rocks).

By adding trace and major element data, this study serves to build upon previous works and provide a higher resolution interpretation of emplacement. An enrichment of U and Th in both breccia pipe and melted country rock relative to the Tamarack intrusion suggests a component of partial melt and incorporation of Thomson metasediments. Similarities in trace element enrichment/depletion trends between melted country rock and breccia pipe matrix also suggest the mixing of melted country rock with Tamarack Intrusion, producing a hybridized magma before brecciation. Silica content averages are higher up-section, and iron oxide weight percent averages are higher down-section. This reflects a progression to more felsic mineralogies at decreasing depths. Major element compositions of felsic minerals in end-of-hole igneous rocks closely resemble those of breccia matrix. Data here supports a previously proposed model of emplacement and explosive hydrothermal brecciation caused by the partial melting and incorporation of hydrous Thomson metasediments. This also confirms a connection between breccia matrix, end-of-hole igneous rocks, and subsequently the Tamarack intrusion.

Enrichment of Cu and Ni in breccia matrices compared to both the end-of-hole igneous rocks and the Tamarack's gabbronorite phase suggests the transport and concentration of these chalcophile elements through hydrothermal fluid movement during brecciation. Linear sulfidic horizons near the Thomson Formation's southern margin may point to a possibility for partial melt interactions with the adjacent Paleoproterozoic Mille Lacs Group intrusions (MRS), in which high sulfide concentrations could crystalize chalcophile elements out of this hydrothermal fluid. Interaction between sulfide rich horizons of the Thomson Formation and magmas similar to the Tamarack may result in changes in chemistry during brecciation, and it is worthwhile to consider that this may point to environments suited to host subsurface breccias and resource potentials.

ACKNOWLEDGEMENTS

I would like to extend immense gratitude to Dr. James Welsh, Dr. Laura Triplet, and Dr. Julie Bartley, and Dr. Jeff Jeremiason all of whom provided me with guidance and support throughout this project. Their insights were integral and given without hesitation. I would like to thank Gustavus Adolphus College for providing me with the necessary facilities, the Rio Tinto Corporation for allowing me to conduct research on their drill core, and Michael Hendrickson for providing the necessary hand samples and thin sections. Finally, I would like to thank my fellow students Russel Krueger, Lindsey Reiners, and Ruby Schaufler for their assistance in lab procedures.

Table of Contents:

I. Introduction

Layered mafic intrusions (LMIs) often boast unique and variable concentrations of economic resources. These deposits exhibit layering from the settling of cumulus minerals within melt, and a continually changing chemical composition resulting from this segregation. Typically primitive in composition, LMIs are often enriched in elements like Cr, V, Cu, Ni, and PGE's, and display increasingly felsic mineralogies moving up-section through their layers. LMIs across Northern Minnesota, such as the Duluth Complex are internationally known for their economic concentrations of Cu-Ni-PGEs. The Tamarack intrusion of Northeastern Minnesota is one such intrusion (LMI) and was discovered by the Rio Tinto Corporation. The processes behind its emplacement are being evaluated in order to determine its economic potential (Hendrickson, 2011). A breccia pipe (L02-02), adjacent, and known to be related to the Tamarack, is economically insignificant, but is being studied here to better understand its depositional history and relationship to the Tamarack body.

Many economic ore bodies including those of uranium, gold, and hydrocarbons can be found in pipe deposits. These deposits are described as steeply plunging subcylindrical bodies that are relatively short in two dimensions compared to the longer third dimension. Pipes commonly form at the intersections of tabular magmatic and structural features such as faults, fissures, dikes, and bedding planes. Like many intrusive formations, they squeeze into weak spaces caused by tectonic and magmatic processes. When exposed at the surface, these pipes can be easily identified as large resistant knobs that display iron staining or chemical signatures of other elements that it hosts. A pipe that contains rock fragments hosted in a fine grained matrix is known as a breccia pipe. Breccias can record chemical influence of an incorporated host rock, and can host unique economic deposits.

Brecciation in pipe deposits can occur through several different processes. Tectonic breccias occur along fault zones when rocks are shattered by large-scale tectonic forces and incorporated into igneous bodies. Brecciated pipes can also form from the ascent of ore-bearing fluids through the Earth's crust. Collapse breccias form as rock, undermined by these fluids, is partially dissolved and collapses or breaks loose, settling into solution caverns. Explosive volatiles may also boil off from rising magma as lower pressures decrease saturation capacities. Explosive Hydrothermal breccias are formed as gases expand at explosive rates; volatiles and rock rush violently upward fragmenting and incorporating country rock that they encounter.

While some of the processes leading to brecciation (explosive volatiles, large scale tectonic forces, and collapse features for example) are understood, some are still considered to be a mystery. Many brecciated deposits involve hydrothermal fluids and are intimately tied to a specific series of events. For example, the emplacement of a kimberlite breccia (Fig. 1) first depends on peridotite magmas being heated deep in the mantle where combined temperatures and pressures can partially melt some of the peridotite, and

potentially create diamonds. Next, volatiles must be added to the magma in order to propel it upward from great depths. As pressures decrease, the magma expands and degasses, rapidly releasing volatiles. This forms an explosive hydrothermal breccia which incorporates broken pieces of country rock as it works its way upward through zones structural and stratigraphic weaknesses. If any one of these steps were missing would the breccia still form, or does it rely more heavily on singular processes? It is typically this progression of events leading to brecciation and emplacement that is poorly understood.

The known relationship between the Tamarack intrusion and its associated graphitic breccia pipe (L02-02) makes this pair of deposits a good opportunity to further study the mechanisms behind brecciation and emplacement. Was there any step that brecciation was particularly contingent on, or were all of the puzzle pieces required to instigate this kind of formation? Can a specific type of brecciated deposit (i.e. explosive hydrothermal brecciation) be associated with LMIs, or only with the specific conditions of this setting?

Chalcophile elements are those that prefer to bond with sulfides rather than silica, like Ni, Cu, and other PGE's. The Thomson Formation contains trace amounts of sulfur within its metasediments (Morey and Ojakangas, 1970), and LMI's like the Tamarack are often Cu, Ni, PGE-rich, so why does pipe L02-02 lack economic concentrations of these chalcophile elements? Are there any missing steps in this setting that would have produced PGE-type mineralization and potentially explain why there is a lack of economic concentrations? By adding trace and major element geochemistry to a previously proposed model of formation (Hendrickson, 2011), this study attempts to answer these types of questions and provide a higher resolution understanding of this subsurface relationship.

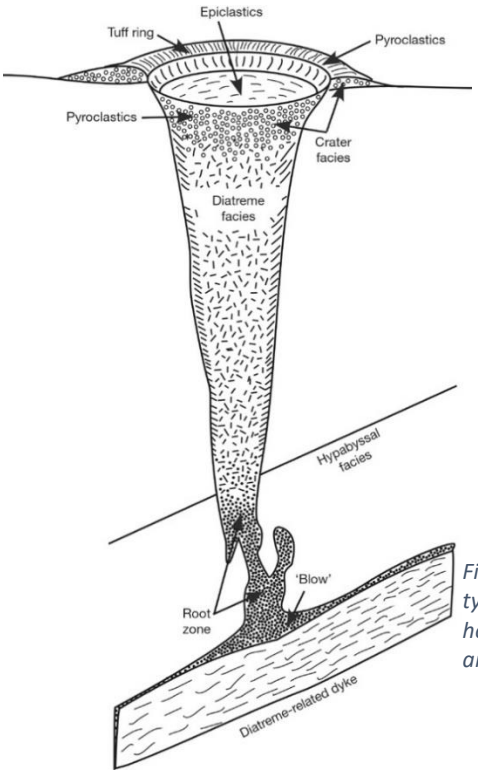

Figure 1 General depiction of a diatreme, one type of breccia pipe deposit. These commonly host diamonds in kimberlite breccias (Wilson and Head, 2007).

II. Geologic Setting

The Tamarack Intrusion, and the associated breccia pipe, were emplaced as intrusive bodies within the Paleoproterozoic Thomson Formation, a slightly sulfidic metasedimentary deposit of the Animikie basin (Fig. 2). This basin formed as a result of the Penokean Orogeny (~1890 Ma) when a mafic suite of rocks was sandwiched between two older, Archean basement formations. The Pembine-Wausau island arc complex was first to collide with the Superior margin. Following this, the collision of Marshfield micro-continent with the Pembine-Wausau terrane instigated mountain building around 1880-1850Ma (Vervoort et al., 2007). These orogenic events created the forland Animikie basin (Fig. 2). Deposition was known to be concurrent with mountain building, and allowed for tectonic compression and the metamorphism of many of these sediments (Schulz et al., 2007). These sediments have been named the Animikie Group, the base of which is the Pokegama Quartzite. The Pokegama is overlain by the Biwabik Iron Formation. Iron formation is subsequently overlain by the Thompson, Virginia, and Rove formations.

Thompson Formation units consist of interbedded argillite, siltstone, and greywacke metamorphosed under lower greenschist facies conditions. These layers are folded to a vertical position with a subvertical and axial planar, slaty cleavage (Boerboom, 2009). Thomson metasediments are known to have trace amounts of recrystallized pyrite within their fine grained matrices, always constituting <3% (Morey and Ojakangas, 1970). However, the Thomson formation is also known to contain linear sulfidic horizons running east to west along its south margin. These consist of large porphryoblasts of cubic pyrite, and are confined to the base of the Thomson (Boerboom et al., 2011). The southern margin of the Thomson Formation borders metabasalts and metagabbros of the Mille Lacs Group (Paleoproterozoic, MRS) (Fig. 3).

Located northeast of both this basin and the study site is the Mesoproterozoic (1100Ma) Mid-Continent Rift System (MRS), comprising a suite of bi-modal tholeiitic rocks (Vervoot et al., 2007). The failed Mid-Continent rift caused the emplacement of the North Shore Volcanic Group, the Duluth Complex, and other satellite intrusions (i.e. the Tamarack intrusion and Mille Lacs Group). The breccia pipe and Tamarack intrusion are thought to be satellite bodies of the most geographically near intrusion: the Duluth Complex. This was emplaced as multiple discrete intrusions below the base of a large volcanic edifice, and is described as having four subdivisions. These include a felsic series, an early gabbro series, an anorthositic series, and a period of LMIs (Severson et al., 2002).

The Tamarack, one of these satellite LMIs, is described as having two layers, the lower of which is a feldspathic lherzolite with coarse grains and olivine cumulates. The upper layer is lherzolite with fine olivine mesocumulates (Goldner, 2011). The Tamarack intrusion is depicted as grey in Figure 4. Surrounding the Tamarack is an assimilation halo, depicted as light pink in Figure 4. The assimilation halo is where the Tamarack intrusion interacted with the surrounding country rock, and comprises the end-of-hole igneous rocks in pipe L02-02. This assimilation halo is particularly important to this study and represents

a step in the progression to a more felsic mineralogy within mafic magmas as they incorporate siliceous sediments through partial melt. The Tamarack Intrusion and its adjacent breccia pipe are located within the southwest portion of the Animike basin (Goldner, 2011) (Fig. 2). The drill core supplied by Rio Tinto Corporation intercepts brecciated rock, Thomson metasediments (depicted as purple in Fig. 4), and assimilated country rock at its lowest depths (end-of-hole-igneous rocks)(Fig. 4). This breccia pipe contains clasts of graphite hosted within a felsic to intermediate crystalline matrix (Appendix 2). In a hypothetical spatial representation of the study site, the breccia pipe intrudes the variably graphitic slate and metagraywacke of the Thomson Formation, and lies adjacent to the assimilated halo of host rock surrounding the Tamarack intrusion (Fig. 3 and 4).

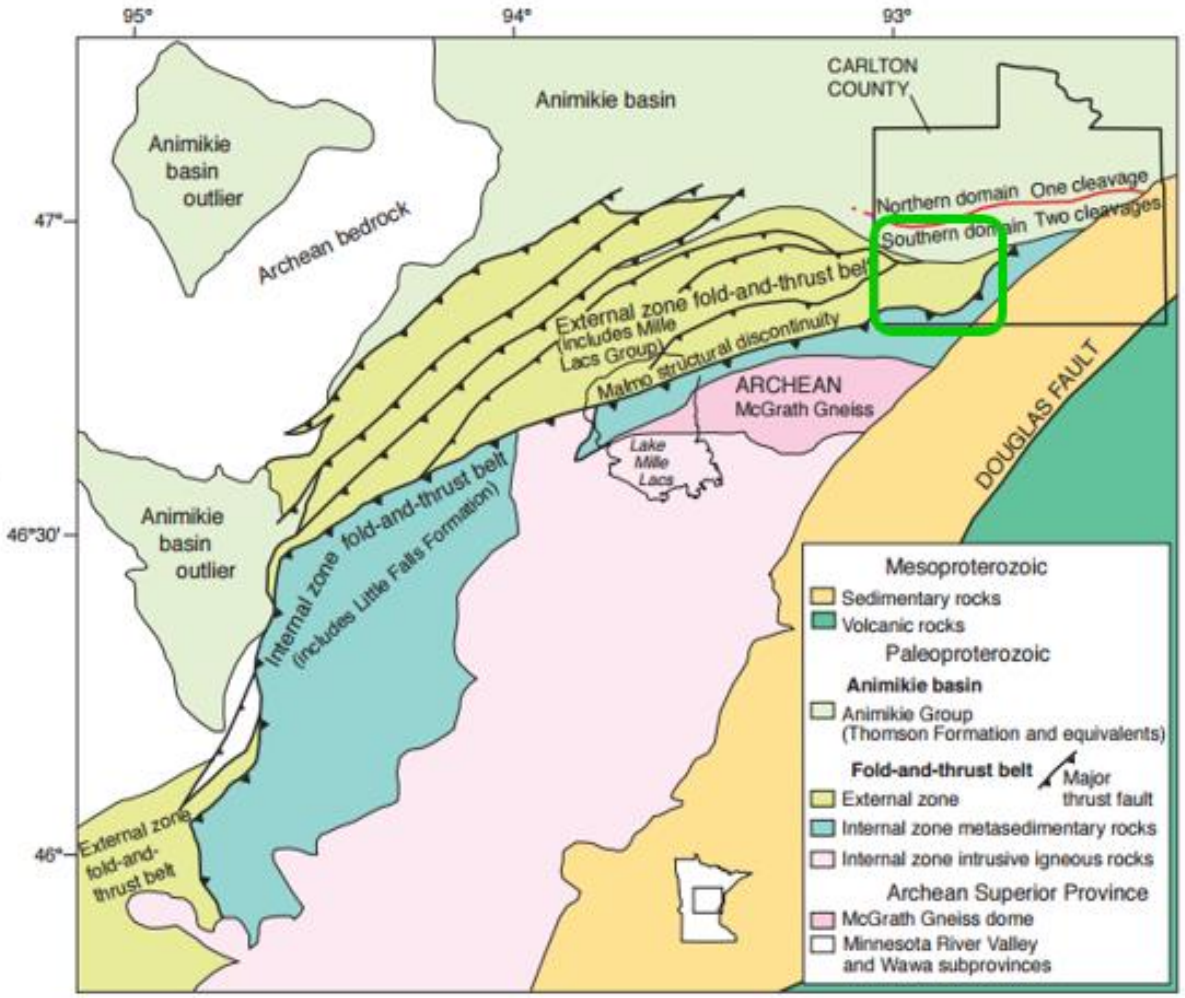

Figure 2 Large scale regional geology and tectonics of Carlton county and surrounding areas (Modified from Boerboom, 2009). Extent and scale of this figure depicted in the small in-set map of Minnesota. Extent of figure 3 outlined in green.

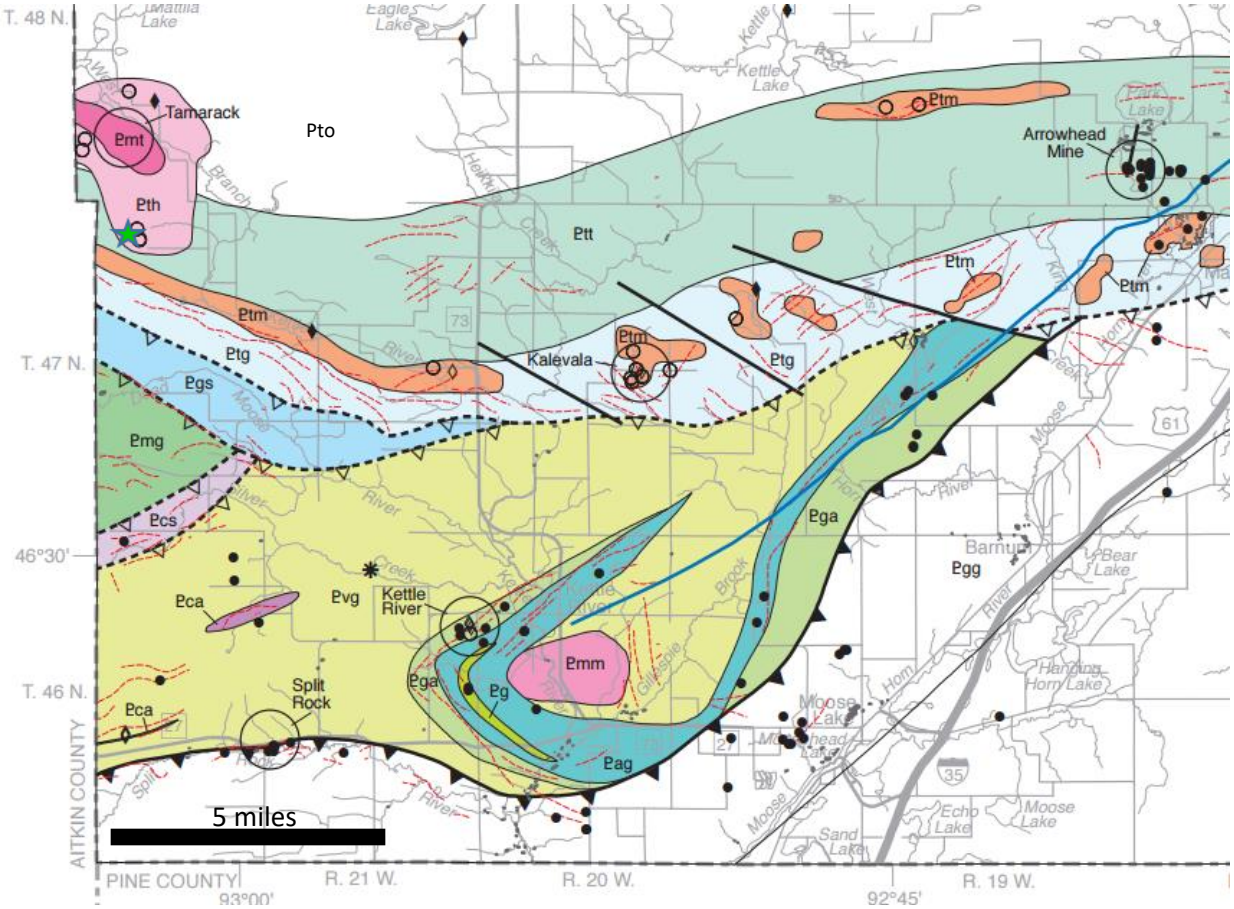

Figure 3: The extent of this figure is outlined in figure 2. The Tamarack intrusion is represented by the dark pink (Pmt) and its surrounding alteration halo by light pink (Pth). This is surrounded by the white in the NW, grey-blue, orange, and light blue representing Thomson formation rocks (Pto, Ptt, Ptm, Ptg), respectively. The location of the drill hole intercepting the core is noted by the green star. The Tamarack intrusion is contained completely within the Thomson formation. The southern rim of the Thomson borders the Mille Lacs Group metagabbros and metabasalts (Pvg, Pmg, and Pga) yellow, dark green, and white in the SE. (Modified from Boerboom, 2009).

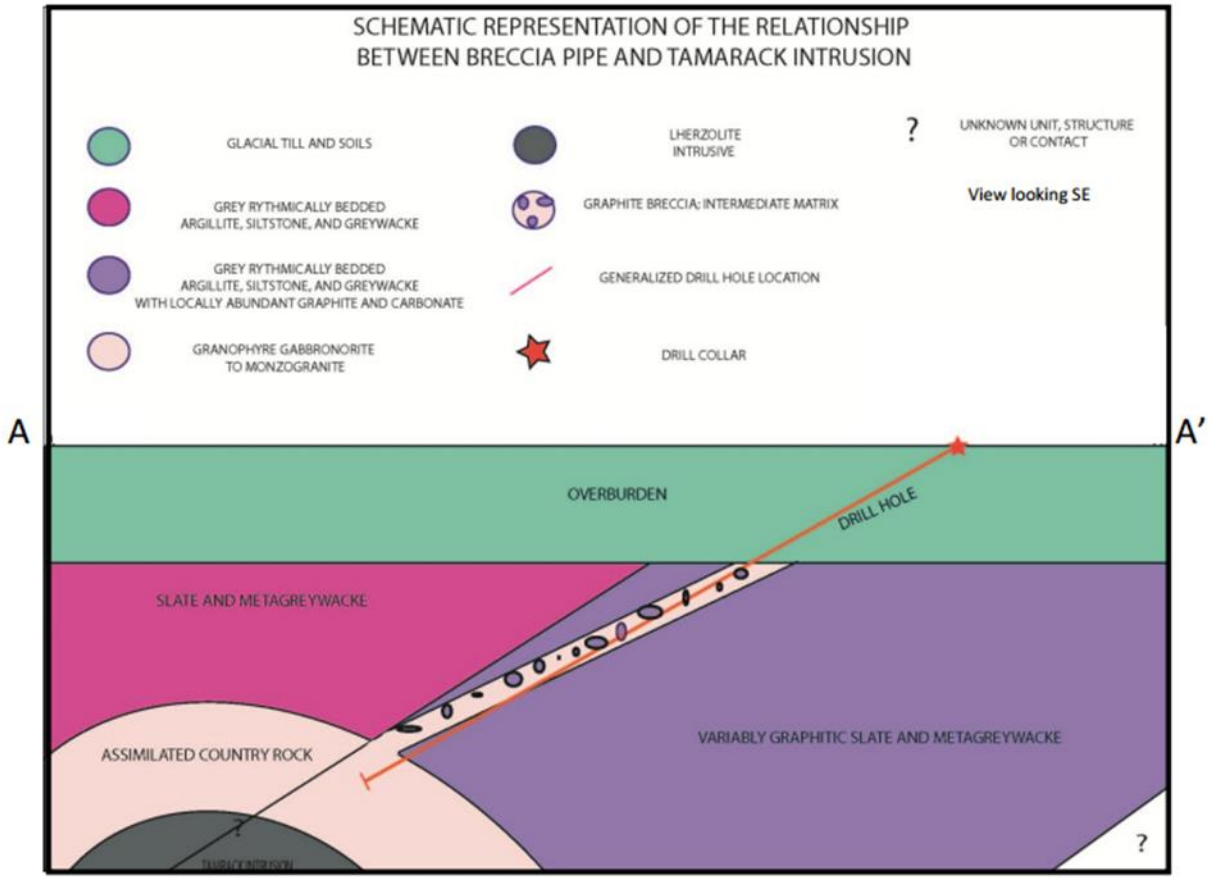

Figure 4: A hypothetical cross-section of the breccia pipe, drill core, and surrounding formations (Hendrickson, 2011)(Modified from Boerboom, 2009) Image not to scale, speculative only. The red line shows the drill pathway. The purple unit represents Thomson metasediments being intruded by the pipe. The Tamarack intrusion is shown in grey, and its assimilation halo is shown in light pink. The view of this cross-section is to the south-east.

III. Previous Works:

Deposit scale descriptions of the Tamarack intrusion are provided by Goldner (2011), and include trace and major element chemistry of the Tamarack intrusion at various depths. Goldner (2011) and Boerboom (2009) also provided spatial relationships depicted in figures 2, 3, 4, and 5, and conclude that the Tamarack is completely contained in the Thomson formation. Regional geology combined with these deposit scale and spatial descriptions led to the conclusion that the Tamarack intruded synchronously with the early stage of rifting in the MRS. The Tamarack intrusion has a shape similar to a tadpole, and is about 13 km long and is between 1 and 4 km wide. The narrow 'tail' area of the tadpole, also the focus of most of the exploration drilling, is composed exclusively of ultramafic rock types. The larger 'body' of the tadpole is at the southeastern end of the intrusion. This is composed of a wider variety of rock types that range from lherzolite to granophyric gabbronorite. This also borders the region of the Tamarack known as the assimilation halo, which was once melted country rock, and is represented by the end-of-hole igneous rocks of core L02-02. The gabbronorite phase is the upper most unit of the Tamarack intrusion and, in particular, its chemistry (Appendix 3) was used as a normalization comparison in my trace element chemical analysis. The gabbronorite is described as a grey, fine to medium-grained, poorly foliated, intergranular rock that is mostly composed of tabular plagioclase, and both granular clinopyroxene, and granular orthopyroxene(Goldner, 2011). Spatial relationships of the Tamarack, gabbronorite, and drill collar of hole L02-02 are depicted in figure 5. (Gabbronorite is discussed more in the methods section).

Hendrickson (2011) studied the breccia pipe, providing thin section and hand sample images (Appendix 1), along with detailed thin section and core descriptions (Appendix 2). Hendrickson (2001) also provided a hypothetical stratigraphic section of the drill hole (Fig. 8). The breccia pipe is characterized by varying sizes of graphitic clasts set in a highly altered matrix. Its matrix is composed mainly of chlorite, sericite, and clays (Appendix 2). At its depths, the drill core also makes contact with end-of-hole igneous rocks, the melted country rocks of the Tamaracks assimilation halo (Hendrickson, 2011). Lithologies and modal percentages of the end-of-hole igneous rocks show increasing percentages of felsic compositions up-section (Fig. 6). Petrographic images display a similar crystal orientation among both breccia and end-of-hole rock (Fig. 7). Hendrickson (2011) was able to rule out a passive model of brecciation where relatively inactive magma rose and dislodged graphitic country rock while incorporating them as inclusions. In such a model, brecciation and emplacement would result directly from the intrusion of the ultra-mafic and mafic Tamarack magmas. This possibility was ruled out because of the more felsic mineralogy of the breccia matrix. Hendrickson proposed that intrusion of the magma into hydrous sediments (Thomson Formation) initiated partial melt and incorporation of volatiles. Eventually, an explosive release of volatiles fractured and emplaced a brecciated pipe in Thomson host rock. It was concluded that igneous end-of-hole rocks formed during or shortly after the intrusion of the Tamarack, and that the melting of metasediments, whose melting temperatures were lowered by high volatile contents, was a primary cause of brecciation (Hendrickson, 2011).

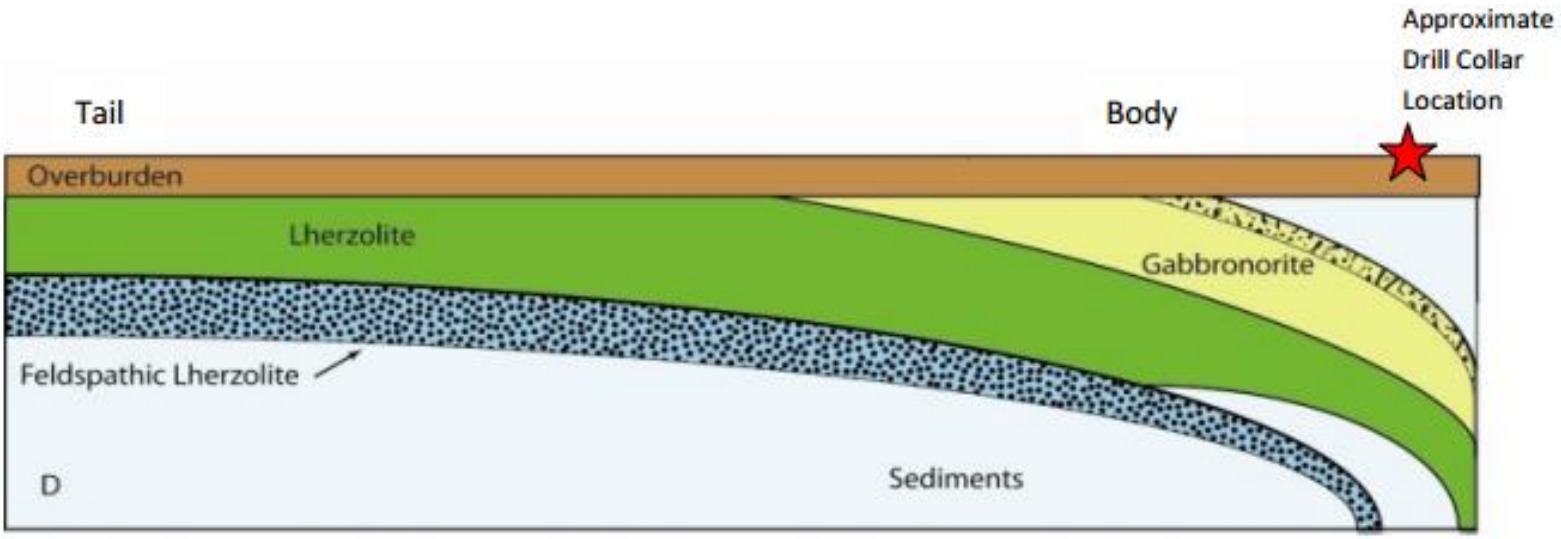

Figure 5 Cross-section depicting the relationship of Tamarack layers and the assimilation halo. Gabbronorite, depicted in yellow, lies at the top of the Tamarack intrusion. (Goldner, 2011)

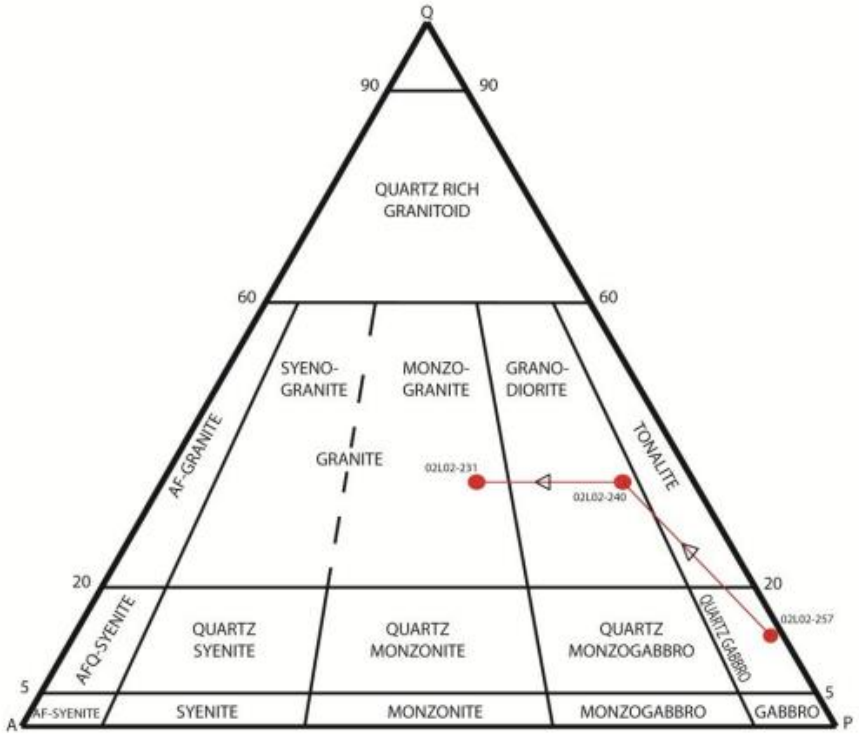

Figure 6 QAP diagram depicting the lithologies and progression of the igneous end-of-hole rocks moving up section. There is an increase of felsic mineralogies up section. (Hendrickson, 2011).

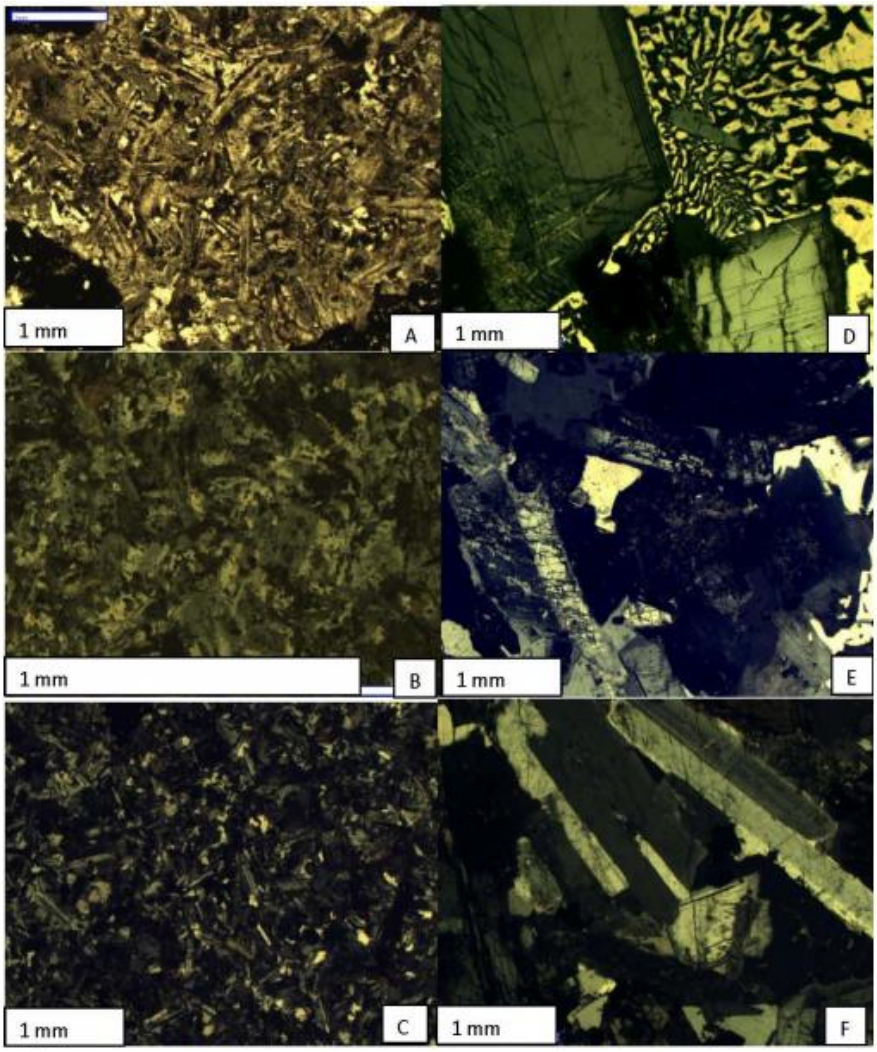

Figure 7 Breccia Matrix is represented by A,B, and C. While end-of-hole igneous textures represented by D,E, and F. Comparison of crystal alignment shows similar orientations between breccia matrix and end-of-hole rocks (Hendrickson, 2011).

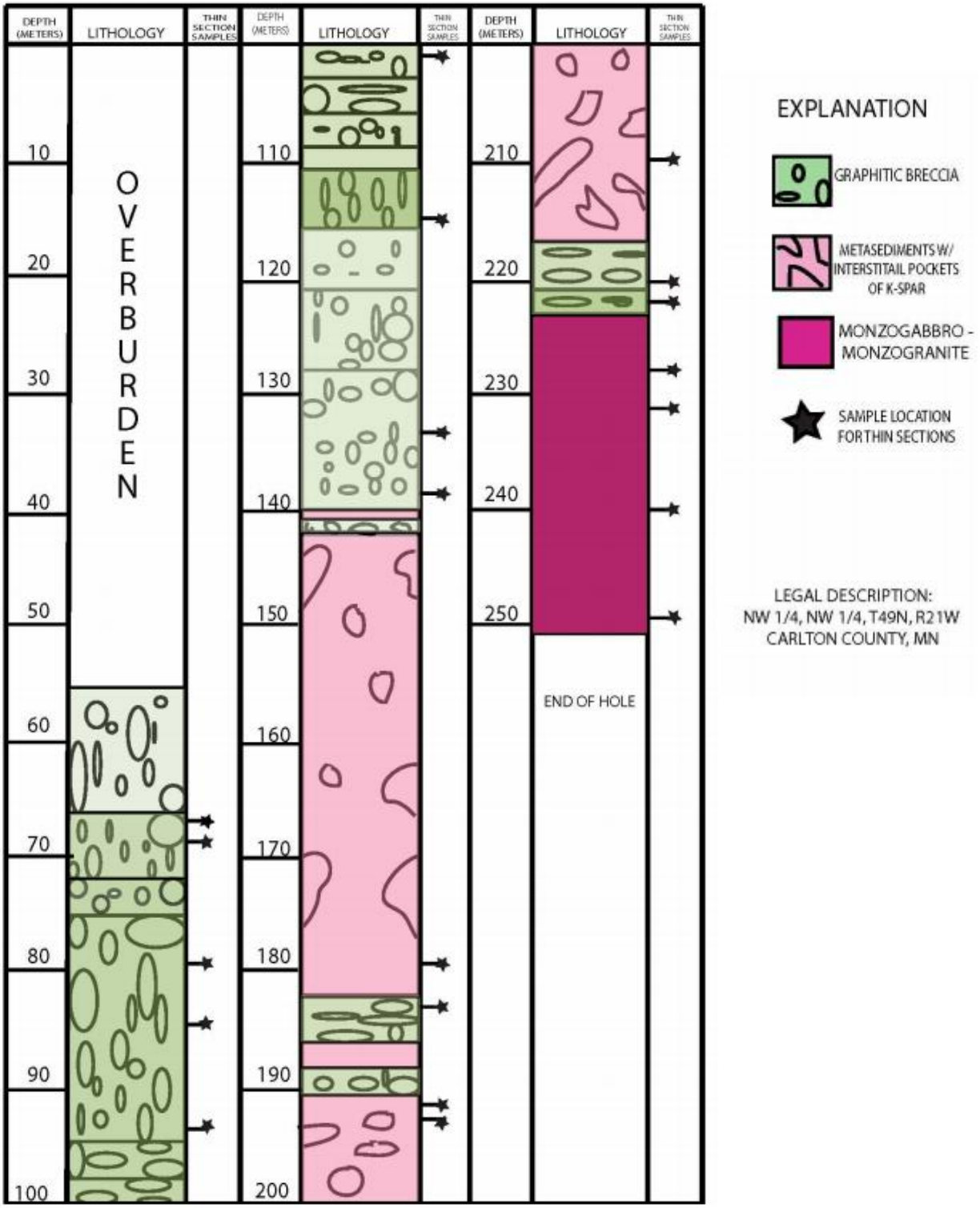

Figure 8 Core log (hole L02-02) of breccia pipe. Detailed core descriptions in Appendix 2. Light shades of green indicate intense alteration of the breccia matrix, darker shades of green indicate less intense alteration of the breccia matrix. Light pink represents metasediments, and dark pink represents the end-of-hole igneous rocks. This core log is for schematic purposes only. (Hendrickson, 2011).

IV. Methods

Samples for this project were collected from drill core supplied by Rio Tinto Corporation to the MNDNR Core Library in Hibbing, MN. Twenty associated thin sections have been cut from both the breccia and assimilated country rock, and anomalous areas within major and proximal lithologies (i.e. reaction rims and metasediments) (Appendix 1). Sample collection and thin section preparation was originally completed by Michael Hendrickson (Hendrickson, 2011).

Breccia matrix samples for this project were collected from depths (in meters) of 133m, 139m, 179m, 192m, 221m, and 222m, and two metasediment samples were collected at 179m and 210m. These were powdered using a micro drill. Samples of end-of-hole igneous rock were collected at depths of 228m, 228m(2), 231m, 240m, 240m(2), and 257m, and were powdered using a ball mill. Representative samples of the end-of-hole samples were powdered this way because the crystal/grain size is too large in order for a micro drill to be reliable. Previously determined modal percentages and the authors discretion was used in selecting representative portions of these phaneritic rocks. Samples were reduced completely to powder to ensure total homogeneity of the representative portion, and the ball mill was thoroughly cleaned using DI water and acetone between runs.

Samples were prepared as follows: 0.13g of each powdered sample was added to a graphite crucible, then 0.75g of lithium metaborate flux was added to each crucible to aid in the fusion process. Samples were then heated in a high temperature furnace at 1000-1050°C for 10-12 minutes in order to form a glass. Only three samples were heated at a time in order to minimize heat loss during transfers. Molten samples were each quickly transferred to propylene bottles containing 61.5g of 1M HNO_3 spiked with internal standard 71-D. In order to fully digest the samples, it was necessary to mechanically shake each for several minutes, in this case, by hand. From there, each sample was diluted 1:200 with non-spiked 2% HNO_3. Calibration standards were made using a concentration range of 1ppb-50ppb. Samples were diluted in this process, so it is necessary to revert these values back to 'original' concentration. Standard major elements (Ca, Ti, Fe, Na, Mg, Al, K, and Mn) were chosen for analysis, and trace and chalcophile elements (V, Ni, Co, Cu, As, Rb, Sr, Ba, Th, and U) were chosen because their concentrations can be very indicative of magma progression, compatibility of melts, and economic resource concentrations. Measured trace and chalcophile elements were also limited to any chosen elements in the work of Goldner's gabbronorite (Appendix 3), in order to ensure that normalization standards were available.

Post ICP-MS dilution calculation:

(mass of rock sample/(mass of water + mass of lithium metaborate + mass of rock sample))*(dilution factor)*(diluted ppb of element)

(1.3*10^-7g/(6.15*10^-5g+1.3*10^-7g+7.5*10^-7g))*200*(diluted ppb of element)

Trace element compositions were normalized as a ratio to the composition of the gabbronorite of the upper Tamarack intrusion. The gabbronorite was chosen for this comparison because of its position within the upper Tamarack; just beneath the assimilation halo (i.e. end-of-hole igneous rocks) (Fig. 5) and above the lower lherzolite of the Tamarack. The assimilation halo is representative of where the Tamarack intrusion was interacting with surrounding country rock. So, a rock in between the boundary of the lower lherzolite and the assimilation halo (i.e. gabbronorite) likely represents a composition similar to the rocks preceding both the end-of-hole igneous rocks and breccia. Major element results were converted to weight percent and multiplied by their respective coefficients (James Cook University, Australia) to convert to weight percent by oxides. There were no measurements taken for silica content so this value was estimated. Silica can be hard to quantify accurately without the proper lab equipment. Glass lab wear, composed of silica, can contaminate samples with enough SiO_2 to make results unreliable. So, silica weight percents were estimated by difference; subtracting the major element weight percents and volatile content from one hundred. Percentage of volatiles (H20 + CO2) in varying stages of the Tamarack intrusion range from 1% to 1.7% (Goldner, 2011). The volatile concentration of breccia matrix and end-of-hole igneous rocks was not actually measured, so this amount was estimated under the assumption that partial melting of hydrated sediments and the incorporation of volatiles occurred. This was done by assuming the lower end of the range to be 2% (higher than the Tamarack's gabbronorite), and giving a generous four percent to set the range's top end member to 6%. Silica weight percent ranges could then be calculated by difference, as mentioned above.

V. Results

Weight percent by oxides are depicted in table 1. Sample 228m(2) represents the sampling of an isolated granitic patch from the chloritized monzogranite that may represent compositions of the partial melt. This is reflected by the abundance of potassium in this sample compared to all other samples, and a stronger similarity to the compositions of breccia matrix rather than end-of-hole igneous rocks. The calculated silica contents of the breccia matrix range from 51.3% to 72.7%, and have an average of 59.1%. Within end-of-hole igneous rocks, the calculated silica weight percent ranges from 45.5% to 66.1%, and have an average of 56.1% when excluding sample 228(2). Average iron oxide weight percents are lower in the breccia matrices than the average in end-of-hole igneous samples, at 10.6% and 12.5% percent respectively when excluding sample 228(2). This exclusion was done because of sample 228(2)'s inferred felsic composition. Without the discussed exclusion, the iron oxide weight percent average of end-of-hole igneous rocks is 10.9%. This supports previous results that the mineralogy of this core becomes increasingly felsic when moving up section (Hendrickson, 2011).

Raw trace element data are reported in tables 2 and 3. All end-of-hole igneous rocks (i.e. assimilated country rock at the lowest depths of drill core L02-02) display similar enrichment and depletion trends (Fig. 9). All rock samples display approximately ten times more uranium and thorium than what is found in the Tamarack body gabbronorite. This is

also true for the concentration of rubidium in every end-of-hole sample (Fig. 9). Each sample has slightly more nickel and rubidium, and slightly less copper than the gabbronorite used for normalization. All samples have considerably depleted strontium concentrations relative to the gabbronorite. Uranium, thorium, and strontium roughly show an increasing magnitude of enrichment/depletion in all samples moving up section through the core (Fig. 9).

All breccia matrix samples show very similar trends in enrichment and depletion of trace elements. Breccia matrix chemistry shows significant enrichment in nickel, rubidium, thorium and uranium relative to the gabbronorite in the Tamarack's assimilation halo (Fig. 10). Despite slightly higher concentrations of nickel, copper, and uranium in the breccia matrix, the trace element chemistry of both matrix and end-of-hole igneous rocks are strikingly similar (Fig. 9 and 10). Raw trace element concentrations are depicted in tables 1 and 2.

Depth (m)	CaO	TiO_2	FeO	Na_2O	MgO	Al_2O_3	K_20	MnO	H_2O +CO_2	SiO_2
133	2.8	1.68	13.47	2.31	2.40	8.82	3.43	0.12	2-6	62.1-58.1
139	3.48	2.11	14.20	2.26	3.00	10.49	3.64	0.03	2-6	57.8-53.8
139(2)	1.84	1.31	9.56	2.78	1.94	21.08	4.17	0.02	2-6	55.3-51.3
192	13.84	1.84	9.80	2.73	2.10	9.11	2.28	0.10	2-6	56.2-52.2
221	7.91	1.91	9.48	1.70	1.50	9.61	3.53	0.08	2-6	62.3-58.3
222	1.60	1.29	8.26	1.78	2.18	7.05	3.08	0.04	2-6	72.7-68.7
179	1.99	1.13	8.09	2.61	1.60	19.78	3.47	0.03	2-6	59.3-55.3
228	4.47	5.04	18.17	2.23	2.13	9.95	4.11	0.12	2-6	51.8-47.8
228(2)	1.54	0.16	1.16	2.39	0.25	16.15	6.64	0.01	2-6	69.7-65.7
231	5.84	0.60	4.56	3.17	0.50	12.97	4.20	0.04	2-6	66.1-62.1
240	6.89	2.32	11.94	2.71	1.18	11.09	3.43	0.09	2-6	58.3-54.3
240(2)	7.95	2.25	11.98	2.51	1.15	12.30	2.74	0.11	2-6	57.0-53.0
257	9.87	3.39	15.73	2.83	0.87	8.10	2.62	0.10	2-6	54.5-51.5
257(2)	9.99	2.95	12.65	2.83	0.80	16.58	2.61	0.09	2-6	49.5-45.5

Table 1 Depicts major element weight percent by oxides of each sample. Yellow (Depths 133-222m) indicates samples taken from breccia matrices, and red (Depth 179m) represents Thomson metasediments. Blue (Depths 228-257m) represents samples taken from end-of-hole igneous rocks. Samples with '(2)' after their label indicate a second sample taken from the same rock.

Depth (m)	51 V	53 V	58 Ni	Co	60 Ni	63 Cu	65 Cu
133	297.4	554.7	445.0	35.4	331.0	103.1	100.7
139	335.4	818.1	530.2	37.1	425.5	94.2	91.8
139(2)	282.9	796.1	364.6	26.8	294.7	72.8	71.0
179	253.2	832.2	209.5	30.0	152.8	52.1	50.8
192	315.7	1160.5	344.9	64.0	267.5	50.5	48.5
221	320.6	1183.8	386.3	35.3	326.5	84.8	82.5
222	285.0	1124.8	325.9	41.7	265.6	46.3	45.9
228	251.5	988.7	295.7	26.7	92.2	36.2	37.2
228(2)	196.7	1003.6	93.6	18.3	89.4	29.3	29.8
231	207.1	1176.3	131.9	16.0	85.3	32.5	31.5
257(2)	210.7	939.0	226.0	22.2	84.9	30.7	30.6
257	216.3	921.2	259.4	24.3	81.7	33.5	32.9

Table 2 Depicts trace element concentrations for the elements V, Ni, Co, and Cu in ppm. Samples with '(2)' after their label indicate a second sample taken from the same rock.

Depth (m)	75 As	77 As	Rb	Sr	Ba	Th	U
133	5.0	190.3	61.8	3.9	203.6	5.3	30.5
139	5.7	430.4	82.2	5.7	375.1	5.9	40.2
139(2)	6.0	577.9	67.3	3.5	266.1	5.7	35.7
179	4.3	765.5	83.6	9.1	430.6	3.9	16.3
192	7.8	794.7	40.1	19.0	330.6	3.6	17.8
221	4.1	962.6	80.5	10.0	374.1	5.4	27.9
222	5.5	971.9	66.4	3.9	275.4	4.1	19.8
228	4.6	991.9	50.9	5.7	463.1	9.6	19.1
228(2)	4.3	1039.0	97.3	6.5	1305.1	10.0	17.1
231	4.0	970.8	84.0	13.3	680.6	6.5	20.8
257(2)	4.2	932.7	53.9	17.0	375.2	4.7	12.3
257	5.3	865.5	51.5	17.1	3849	4.2	10.4
240(2)	4.4	828.2	39.8	11.0	299.7	4.0	7.2
240	4.5	756.0	51.5	11.8	546.9	4.2	10.6

Table 3 Depicts trace element concentrations for the elements As, Rb, Sr, Ba, Th, and U. Samples with '(2)' after their lable indicate a second sample taken from the same rock, at the same depth.

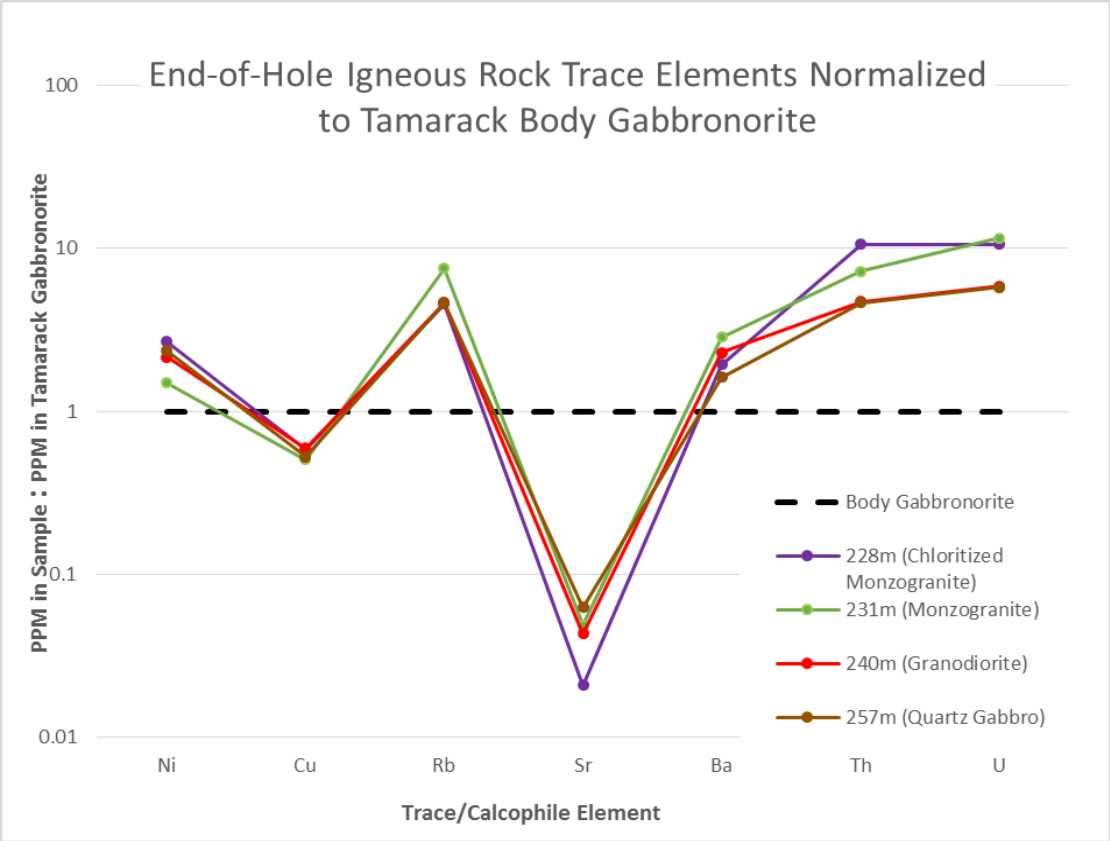

Figure 9 Spider plot depicting trace and chalcophile elements in the end-of-hole igneous rock as a ratio of ppm in each rock sample to an average concentration of that element in the Tamarack intrusion. Averages were taken from the work of Goldner (2011), and the body Gabbronorite was chosen because it represents a late stage of the Tamarack intrusion in its assimilation halo. Numbers (i.e. 228m) represent depth in meters within the drill core.

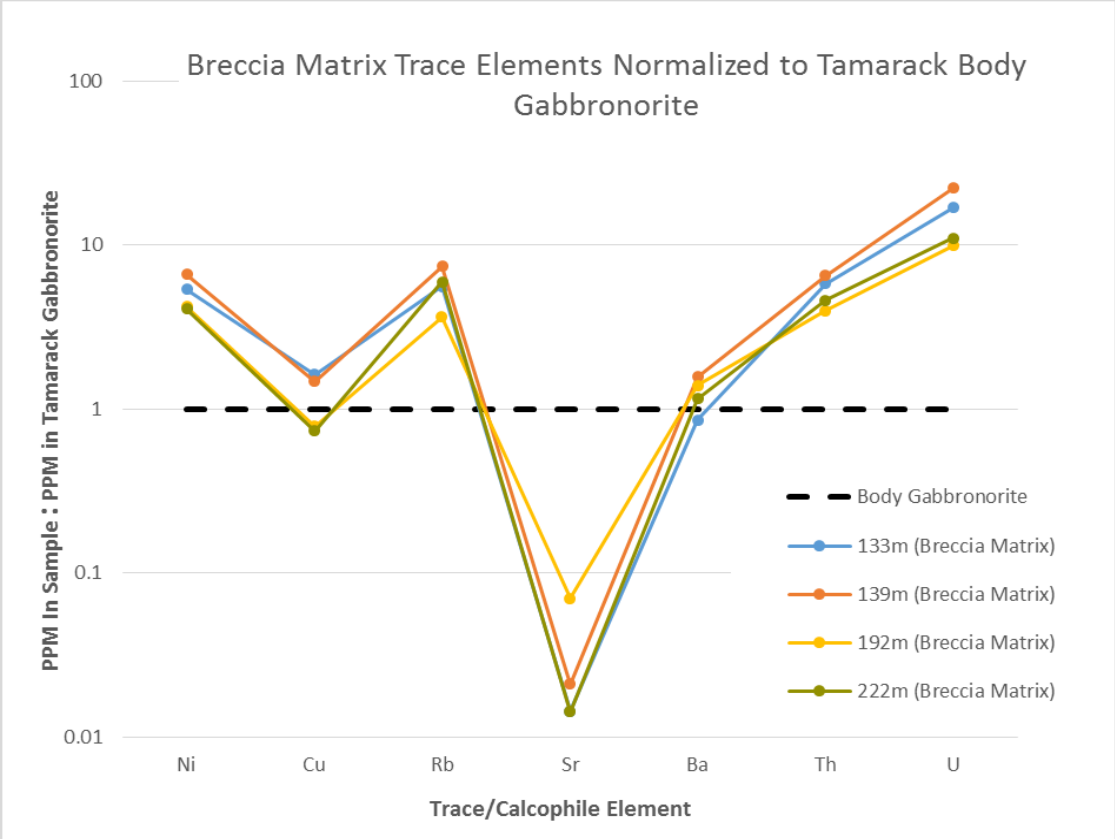

Figure 9 Spider plot depicting trace and chalcophile elements in the breccia matrix as a ratio of ppm in each rock sample to an average concentration of that element in the Tamarack intrusion. Averages were taken from the work of Goldner (2011), and the body gabbronorite was chosen because it represents a late stage of the Tamarack intrusion in its assimilation halo. Numbers (i.e. 133m) represent depth in meters within the drill core.

VI. Discussion

Emplacement and Brecciation

Strong similarities exist among trace element enrichment and depletion trends of breccia pipe matrix and end-of-hole igneous rocks, indicating a partial melt component within the assimilation halo. Partial melt is also suggested by elevated levels of late stage elements, uranium and thorium in both breccia matrix and end-of-hole igneous rocks, relative to the Tamarack gabbronorite. U and Th have increasing compatibilities in melt as silica and highly charged cations such as Na and Al are added from the sediments being incorporated. There are major element similarities between breccia matrix and 228m(2) (previously discussed in the methods section), and major element dissimilarities between 228m(2) and overall end-of-hole rock composition. This may indicate the addition of this type of felsic material into melt during the interaction of the assimilation halo and Thomson sediments before brecciation. This is potentially what has driven the progression toward the felsic mineralogies seen in breccia matrices. An increasingly felsic mineralogy caused by the partial melt and incorporation of this type of material from Thomson sediments have increased the compatibility of late stage elements, U and Th.

Connecting breccia pipe matrix to end-of-hole igneous rocks, and subsequently the Tamarack, confirms the work of Hendrickson (2011). Emplacement of the breccia pipe likely occurred simultaneously with or after the intrusion of the Tamarack. Also, the melting of hydrous metasediments in contact with the Tamarack's assimilation halo likely instigated brecciation. As more volatiles were continuously incorporated, this hybrid magma likely surpassed the energy threshold of the Thomson metasediments and caused an explosive brecciation. However, the hybrid magma was likely created before brecciation, and this is what comprises the breccia matrix. These results also suggest that incorporated clasts of graphitic metasediments had little impact on the chemistry of the breccia matrix during brecciation.

So, was brecciation contingent on any one step or process? Can explosive hydrothermal breccias and LMI's be associated? The incorporation of volatiles such as H_2O and CO_2 through the partial melt of hydrated sediments seems to be the most important mechanism when forming an explosive hydrothermal breccia in these shallow subsurface settings. Other variables, such as the parent magma of the intrusion (i.e. the Tamarack) or how these sediments were introduced to the melt, seem like they could be swapped with another process. LMI's and explosive hydrothermal breccias cannot be directly associated. However, as long as hot magma encounters hydrated sediments with low enough melting points, partial melt will incorporate volatiles, increase the energy of the melt, and likely lead to brecciation.

Economic Mineralization and Exploration

Breccia pipe matrices are enriched in Cu and Ni compared to both the Tamarack's gabbronorite and the end-of-hole igneous rocks of the assimilation halo, so, these

chalcophile elements are definitely being transported and concentrated in breccia matrices. This is likely because they are incompatible in siliceous melt, being picked up by volatiles and hydrothermal fluid, and deposited during brecciation. Sulfide minerals are also present in the Thomson formation both as trace amounts of pyrite crystals in the metasedimentary units (Morey and Ojakangis, 1970) and, along its southern margin, as large porphyroblastic pyrite cubes (Boerboom et al., 2011).

So, can anything explain why there is no economic mineralization seen within pipe L02-02? There are several factors that could have prevented this type of mineralization. There may not have been high enough concentrations of Cu, Ni, and PGE's in the intruding magma or hydrothermal fluid to produce economic concentrations. There also may not have been enough sulfur in the Thomson formation to change chemistry during brecciation and mineralize these chalcophile elements. Sulfur content was not measured in this study, and could be very useful in determining degrees of sulfide incorporation and the origin of sulfide minerals in breccia matrices.

Can this point to a place where brecciation could have produced economic mineralization? There are linear sulfide-rich horizons within the Thomson southern margin that border the Mille Lacs Group metabasalts and metagabbros (Paleoproterozoic, MRS) (Fig. 3)(Boerboom et al., 2011). These linear horizons contain much higher sulfur concentrations than the rest of the Thomson Formation, and the Mille Lacs group rocks are mafic and of a similar age to the Tamarack. The proximity of these features provide definite potential for a similar hydrothermal brecciation as breccia L02-02. If brecciation were instigated and passed through these zones, some of the incorporated clasts would likely be sulfide-rich, instead of the graphite clasts typical of incorporated Thomson formation. High enough sulfur concentrations could potentially pull chalcophile elements from hydrothermal fluids, and unlike breccia L02-02, change chemistry during brecciation. The south rim of the Thomson formation has the potential for both explosive hydrothermal brecciation, and economic concentrations of Cu, Ni, and PGE's within proximal intrusions of the MRS (i.e. Mille Lacs Group).

The breccia pipe discovered by the Rio Tinto is not economically mineralized; however, brecciated deposits in analogous settings at least have the potential to host economic concentrations of sulfide minerals. While this does not definitively point to any new resource potentials, it does emphasize the importance of studying brecciated deposits. It is worthwhile to consider that there may be subsurface breccias currently unavailable for extraction, and that studies such as this may point to environments suited to host them.

References cited:

Boerboom, T.J. 2009. County atlas series atlas C-19, PART A Plates 2&6—Bedrock Geology. Minnesota Geological Survey, 1 p. (map).

Boerboom, T.J., Holm, D., Van Shumas, R. 2011. Late Paleoproterozoic Deformational, Metamorphic, and Magmatic History of East-Central Minnesota. The Geological Society of America, Field Guide 24, 1-25.

Chandler, V. W., Boerboom, T.J., Jirsa, M.A. 2007. Penokean Tectonics Along a Promontory Embayment Margin in East-Central Minnesota. Precambrian Research, 157, 26-49.

Goldner, B.D. 2011. Petrology of the Ni-Cu-PGE mineralized Tamarack Intrusion, Aitkin and Carlton Counties, Minnesota. Masters Thesis, University of Minnesota, 1-151.

Hendrickson, M. 2011. Petrologic Investigation of a Graphitic Breccia Pipe in Proximity to the Tamarack Cu-Ni-PGE Deposit; Carlton County, Minnesota, Gustavus Adolphus Geology Department.

Hutchinson, C. H. 1983. Economic Deposits and their Tectonic Setting. John Wiley and Sons, Inc., New York, 104.

James Cook University, Analytical Center, Australia, Element-to-Stoichiometric Oxide Conversion Factors. Retreived from:

https://www.jcu.edu.au/advanced-analytical-centre/services-and-resources/resources-and-extras/element-to-stoichiometric-oxide-conversion-factors

Morey, G.B., and R.W. Ojakangas. 1970. Sedimentology of the Middle Precambrian Thomson Formation, East-Central Minnesota. Minnesota Geological Survey, Report of Investigations 23, 1-29.

Schulz, K. J., Cannon, William F. 2007. The Penokean Orogeny in the Lake Superior region. Precambrian Research, 157, 4-25.

Severson, M.J., Miller, J.D., Peterson, D.M., Green, J.C., and Hauck, S.A., 2002. Mineral Potential of the Duluth Complex and Related Intrusions, Minnesota Geological Surv. Report of Investigations 58, p. 164-200.

Vervoort, J. D., Wirth, K., Kennedy, B., Sandland, T., Harpp, K.S. 2007. The Magmatic Evolution of the Midcontinent Rift; New Geochronologic and Geochemical Evidence from Felsic Magmatism. Precambrian Research, 157, 235-268.

Appendix 1: Core Photos; Hand Sample and Thin Section

Figure 11 Hand sample photos taken by Michael Hendrickson (2011) at the MNDNR Core Storage Facility in Hibbing, MN.

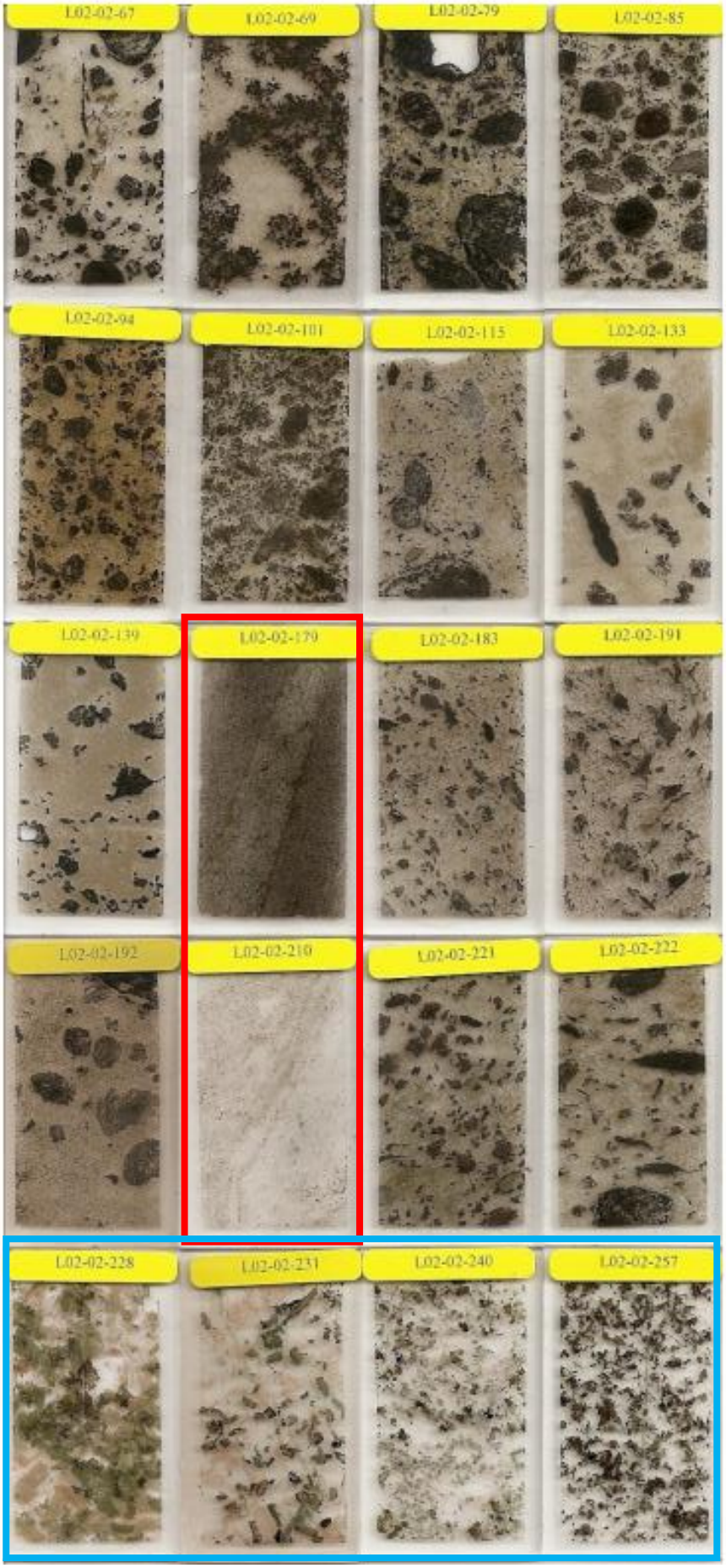

Figure 12 Thin section pictures at various depths within drill core L02-02. End-of-hole igneous rocks are outlined in blue, metasediments are outlined in red, and all other images represent breccia pipe. Last number in each label corresponds to depth in meters. Thin section descriptions provided in Appendix 2 (Hendrickson, 2011).

Appendix 2: Thin Section Descriptions (Hendrickson, 2011)

All thin section descriptions were written by Michael Hendrickson (2011). Done using normalized point counts.

LO2-02-67-Breccia: Light green to black, graphite dominated.

5% yellow to silver anhedral pyrite 1mm-5mm diameter clustered in graphite clasts - 25% black poikioblastic graphite clasts that are subhedral ranging in diameter from 1mm-4mm - 70% intermediate to felsic matrix that is light tan to green color.

LO2-02-69-Breccia: Light green to black, graphite dominated, with an intermediate to felsic matrix.

<5% yellow pyrite as .5-1mm pyritihedrons or cubes - 10% yellow to orange alteration mineral (epidote?) surrounding graphite clasts - 40% anhedral and skeletal black graphite clasts 1mm-10m diameter - 40% light green intermediate to felsic matrix, that contains black euhedral laths 1-2mm long and .25-.5mm wide - The matrix appears to be highly altered.

L02-02-79-Breccia: Green to black hosting black graphite clasts.

60% black anhedral and poikioblastic graphite clasts .5mm-20mm in diameter - 40% light green to dark green matrix of felsic to intermediate composition.

L02-02-85-Breccia: Black to green hosting graphite clasts.

<1% anhedral hematite masses, 1mm in diameter within graphite clasts - 50% green matrix of felsic to intermediate mineralogy - 50% black, 1mm-20mm diameter anhedral-round graphite clasts - Specimen is altered.

L02-02-94-Breccia: Green to black hosting graphite clasts

<1% yellow pyrite as <1mm anhedral masses in graphite clasts - 70% brown to green matrix of felsic to intermediate mineralogy with <1mm x .1mm white euhedral laths of unknown mineralogy - 20% anhedral and black 3mm-10mm in diameter graphite clasts.

L02-02-101-Breccia: Black to green, black graphite dominated, with matrix mineralogy ranging from intermediate to felsic.

80% black graphite subhedral to anhedral poikioblastic clasts 1mm-10mm in diameter - 5% yellow to silver pyrite or arsenopyrite as 1 mm cubic or pyritihedron or anhedral masses 3- 45 6mm in diameter - 15% light green intermediate to felsic matrix with white euhedral laths 1-2mm long and .25-.5 mm wide - The matrix is altered.

L02-02-115-Breccia: Green to dark green hosting graphite clasts, and is matrix dominated.

<5% yellow pyrite as anhedral masses in matrix, 1-2mm in diameter - 15% black anhedral and poikioblastic graphite inclusions 1mm-15mm in diameter - 40% green to dark green matrix of alkali to intermediate mineralogy - Minor alteration is also present.

L02-02-133-Breccia: Light green to green and possesses graphite clasts.

15% .5-2cm diameter anhedral to acicular poikioblastic black graphite clasts - <1% yellow, anhedral, and 1mm diameter pyrite within graphite clasts - 90% light green to green matrix of intermediate to felsic mineralogy and crystal geometry - A light green halo surrounds graphite clasts.

L02-02-139-Breccia: Dark green to black with black graphite clasts.

90% dark green matrix of intermediate to felsic 46 mineralogy - 10% 1mm-10 mm in diameter subhedral graphite clasts - <1% yellow pyrite as anhedral masses within graphite clasts.

L02-02-179-Metasediment: Black metasediment.

99% black siliceous metasediments - <1% acicular to subhedral 10mm x 1mm interstitial pockets of K-feldspar.

L02-02-183-Breccia: Black to green containing black graphite clasts.

<1% yellow pyrite in disseminated 1mm anhedral masses within graphite inclusions - 5% ~1mm red anhedral amoeboid interstitial pockets of Kfeldspar - 30% black graphite anhedral to acicular clasts 1-3mm in diameter - 60% green matrix of intermediate to felsic mineralogy.

L02-02-191- Breccia: Black, hosting black graphitic clasts.

<5% yellow pyrite as anhedral masses, 1mm-10mm in diameter, and commonly adjacent to or within graphite clasts - 70% intermediate to felsic matrix - 30% subhedral and poikioblastic 1mm-15mm diameter graphite clasts commonly haloed by unknown mineral - <5% red K-feldspar as anhedral interstitial masses 1-2mm in diameter.

L02-02-192-Breccia: Black to green possessing graphitic clasts.

50% felsic to intermediate matrix - 50% .5-1.5 cm black poikioblastic graphite clasts that are anhedral and surrounded by light green halos of unknown mineralogy - < 5% <1mm anhedral pockets of K-feldspar hosted in metasediments - <1% anhedral masses of yellow pyrite ranging in size from 1-5mm in diameter - < 5% 1mm x .1mm acicular to subhedral yellow/orange mineral commonly found in graphite clasts, andrarely found in matrix

L02-02-210-Metasediment: Black metasedimentary rock with quartz veins.

90% black siliceous metasediments - 10% laterally continuous and parallel segments of red K-feldspar ~3cm long and ~.3cm wide located in bottom right half of sample - <5% quartz as 3cm long and .2cm wide veins spanning top to bottom of sample, along with variably spaced and irregular fracturing present trending EW across specimen.

L02-02-221-Breccia: Dark green with graphite clasts.

<1% yellow anhedral pyrite 1mm in diameter within graphite clasts - 90% felsic to intermediate dark green matrix with <1mm x .1mm acicular white to yellow laths of unknown mineralogy - 15% 1-3mm anhedral to acicular graphite clasts with hematite halos.

L02-02-222-Breccia: Green to dark green to yellow, possesses graphite inclusions, and is matrix dominated.

<5% yellow pyrite as~1mm anhedral masses commonly adjacent to graphite or in graphite clasts - 20% black anhedral graphite clasts ranging in diameter from 1mm-10 mm - <1% pink K-feldspar as<1mm diameter anhedral masses - 90% green to dark green matrix with yellow minerals, representing an intermediate to felsic composition.

L02-02-228-Chloritized Monzogranite: Black to red chlorotized monzogranite.

Nearly no primary plagioclase remaining - 1mm-6mm x 1mm-6mm interstitial anhedral quartz - 2mm-6mm x 3mm-7mm graphic to granophyre textures of K-feldspar and quartz - .25mm-.5mm x 5mm-8mm acicular apatite, .25mm x .25 mm in cross section - .5mm-1mm x .5mm-1mm euhedral to anhedral that are occasionally skeletal opaques - 1mm-5mm x 1mm- 10mm chlorite masses that are anhedral/ sub-hedral and interbolate.

Alteration: Clay, Sericite, Pyrophyllite, Chlorite. Chlorite masses are euhedral to anhedral, .5mm-3mm x .5mm-5mm and interstitial to plagioclase laths. Clay, sericite, and pyrophyllite masses are euhedral to anhedral, 1mm-4mm x 1mm-5mm, replacing plagioclase or K-feldspar.

L02-02-231-Monzogranite: Red to black monzogranite.

2mm-8mm x 1mm-4mm euhedral, inequalgranular and holocrystalline plagioclase laths that are zoned and twinned - 2mm-6mm x 2mm-6mm graphic to granophyre textures of Kfeldspar and quartz - 1mm-4mm x 1mm-3mm anhedral interstitial quartz with amoeboid boundaries.

Alteration: Clay, Sericite, Pyrophyllite, Chlorite. Chlorite masses are euhedral to anhedral, .5mm-1mm x .5mm-2mm and interstitial to plagioclase laths. Clay, sericite, and pyrophyllite masses are euhedral to anhedral, .5mm-1mm x .5mm-1mm, replacing plagioclase or K-feldspar.

LO2-02-240-Granodiorite: Grey to blue to red granodiorite

. .5mm-2mm x 1mm-6mm sub-hedral, zoned and twinned, interlocking, inequalgranular, holocrystalline plagioclase laths with polygonal grain boundaries - 1mm-2mm x 1mm-8mm anhedral quartz - 1mm-2mm x 1mm-2mm graphic/ granophyre texture of quartz and K-feldspar - .5mm-1mm x .5mm-1mm euhedral to anhedral opaques - .5mm-1mm x .5mm-1mm euhedral to anhedral opaques.

Alteration: Clay, Chlorite, Sericite, Pyrophyllite. Chlorite masses are euhedral to anhedral, .5mm-1mm x .5mm-2mm and interstitial to plagioclase laths. Clay, sericite, and pyrophyllite masses are euhedral to anhedral, .5mm-.5mm x .5mm-.5mm, replacing plagioclase or K-feldspar

L02-02-257-Quartz Gabbro: Dark green quartz gabbro.

2mm-5mm x .5mm-1mm zoned and twinned, holocrystalline, inequalgranular, and interlocking plagioclase laths with polygonal grain boundaries - 1mm-3mm x 1mm-3mm amoeboid interstitial quartz and K-spar - 1mm-2mm x 1mm-2mm subhedral biotite - .5mm- 1mm x .5mm-1mm anhedral opaques - 1mm-3mm x 1mm-2mm subhedral amphibole with distinct cleavage - .5mm-1mm x .5mm-1mm subhedral to anhedral augite crystals.

Alteration: Chlorite. Chlorite masses are euhedral to anhedral, .5mm-.5mm x .5mm-.5mm, and interstitial to plagioclase laths.

Appendix 3: Trace Element Geochemistry, Tamarack Intrusion (Goldner, 2011)

The geochemistry of the 'gabbronorite' within Goldner's analysis of the Tamarack was used for normalization. All concentrations in ppb.

Table 3: Body Trace Elements

	Granophyric Gabbronorite								Gabbronorite									
Analyte Symbol	3-58	3-62	3-63	3-71	3-76	3-91	3-97	3-99	3-106	3-120	3-135	3-150	3-161	3-173	3-187	3-191	3-195	3-196	3-202	3-208
Rb	74	130	67	50	45	32	14	41	23	22	13	11	8	8	6	10	28	2	9	5
Ba	788	823	733	588	525	417	263	525	364	337	265	232	182	176	158	207	694	94	171	101
Th	9.5	8.6	8	6.4	5.5	3.9	2.1	6.6	2.9	3.2	2.1	1.9	1.3	1.4	1	1.6	8.2	0.3	1.6	0.7
U	1.9	3.1	1.8	1.5	1.3	1	0.5	1.4	0.7	0.7	0.4	0.3	0.2	0.2	0.2	0.3	1.4	0	0.3	0.1
Nb	19	10	21	21	18	14	6	15	13	11	5	4	3	3	3	4	14	0	4	1
Ta	1.2	0.7	1.3	1.3	1.2	1	0.4	1.1	1	0.6	0.4	0.3	0.2	0.2	0.2	0.2	0.9	0	0.2	0
La	55.5	35.6	51	52	39	33	12.9	34.6	17.2	16.3	15.1	12	9.3	9	7.9	9.9	53.3	2.6	9.8	4.4
Ce	103	70	98.9	103	77.7	64	23.5	64.9	31.2	35.6	26.8	21.9	17.1	17.1	14.9	18.9	97.4	4.7	18.8	8.7
Pb	7	6	8	10	12	10	5	12	7	7	7	5	0	0	0	0	7	0	0	0
Pr	11.3	7.79	11	12	8.9	7.4	2.57	6.96	3.43	3.93	2.78	2.37	1.87	1.9	1.68	2.09	10.8	0.53	2.1	1.03
Sr	224	99	238	235	278	313	324	254	397	379	348	321	290	274	273	264	229	269	213	132
Nd	43.6	27.2	45.3	47	36.6	31	10.7	27.5	13	15	10.9	9.5	7.8	8.1	7	8.7	39.5	2.3	9.3	4.7
Zr	199	124	203	186	193	106	56	180	89	92	65	53	43	45	36	58	214	13	58	26
Hf	6.3	3.4	6	5.6	5.1	3.3	1.9	5	2.6	2.6	2	1.7	1.4	1.5	1.2	1.6	6.1	0.4	1.8	0.9
Sm	10.2	5.7	10.5	11	8.4	7.8	2.6	6.3	2.9	3.3	2.5	2.2	2	2.1	1.7	2.1	8.6	0.6	2.3	1.3
Eu	2.95	1.25	3.08	3.4	3.03	3.2	1.89	2.33	2	2.33	1.38	0.98	0.82	0.72	0.73	0.8	2.4	0.35	0.76	0.48
Gd	9.5	5.1	9.5	10	8.3	7.2	2.5	5.8	2.8	3.2	2.5	2.3	2	2	1.9	2.2	8.6	0.6	2.3	1.3
Tb	1.5	0.8	1.5	1.6	1.2	1.1	0.4	0.9	0.4	0.5	0.4	0.4	0.3	0.3	0.3	0.4	1.3	0.1	0.4	0.2
Dy	8.5	4.4	8.2	8.3	6.7	5.6	2.6	5.2	2.5	2.9	2.3	2.2	2	2	1.8	2.1	7.2	0.6	2.3	1.4
Y	43	22	44	41	35	29	14	29	14	15	13	11	9	11	9	11	38	3	11	3
Ho	1.6	0.9	1.5	1.5	1.3	1	0.5	1	0.5	0.6	0.4	0.4	0.4	0.4	0.4	0.4	1.4	0.1	0.5	0.3
Er	4.3	2.6	4.3	4.1	3.4	2.6	1.4	2.8	1.3	1.6	1.2	1.2	1.1	1.1	1	1.2	3.9	0.4	1.3	0.8
Tm	0.6	0.38	0.59	0.6	0.47	0.4	0.2	0.39	0.19	0.22	0.17	0.17	0.16	0.16	0.14	0.16	0.56	0.06	0.18	0.11
Yb	3.7	2.5	3.5	3.3	2.8	2.1	1.3	2.4	1.2	1.4	1.1	1.1	1	0.9	0.9	1	3.5	0.4	1.1	0.7
Lu	0.53	0.36	0.52	0.5	0.4	0.3	0.22	0.36	0.19	0.21	0.17	0.16	0.15	0.14	0.13	0.15	0.48	0.06	0.16	0.1

Figure 13 Trace Element chemistry of the body gabbronorite within the Tamarack's assimilation halo. Taken from Goldner (2011). Ppb.

Table 5: Body Chalcophile Elements

	Granophyric Gabbronorite								Gabbronorite									
Analyte Symbol	3-58	3-62	3-63	3-71	3-76	3-91	3-97	3-99	3-106	3-120	3-135	3-150	3-161	3-173	3-187	3-191	3-195	3-196	3-202	3-208
Au	3	1	0	0	0	0	0	3	3	3	0	0	0	2	0	0	0	2	0	0
Pt	8.2	2.3	8.9	0.4	0.3	0	7.5	0	0.4	0	0.5	2.1	0.9	7.6	0.7	7.3	0.7	1.6	0.2	5.6
Pd	0	2.9	0	0	0	0	0.2	0	0.1	0	0.3	1.5	0.6	0	0.4	0	0	1.4	0	3
Ni	1	88	5	5	7	19	62	18	33	30	45	86	70	100	153	92	24	363	144	486
Cu	19	16	18	21	20	18	27	34	18	16	7	101	91	109	198	60	50	322	87	405
Ag	0.3	0	0	0.3	0	0	0	0	0	0	0	0	0	0	0	0	0	0	0	0
S	300	660	250	470	900	1030	1340	2290	1960	1270	1530	2130	1480	1530	1810	960	970	1530	1000	2930

Figure 14 Chalcophile trace element chemistry of the gabbronorite within the Tamarack's assimilation halo. Taken from Goldner (2011). Ppb.